



# Electric Double-Layer Capacitance of Meso/Macroporous Activated Carbon Fibers Prepared by the Blending Method

## I. Nickel-Loaded Activated Carbon Fibers in Propylene Carbonate Solution Containing LiClO<sub>4</sub> Salt

Soshi Shiraishi,<sup>\*,z</sup> Hideyuki Kurihara, Lan Shi, Takuya Nakayama, and Asao Oya

Department of Chemistry, Faculty of Engineering, Gunma University, Kiryu, Gunma 376-8515, Japan

Meso/macroporous activated carbon fibers (ACFs), containing mesopores and macropores in addition to micropores, were prepared from carbonization and steam-activation of the phenolic resin fibers blended with a small amount (0.1 wt %) of an organic nickel complex. Conventional (microporous) ACF as reference sample, mainly composed of micropores, was also prepared from pure phenolic resin fibers without any agent. The electric double-layer capacitance of these ACFs was measured in propylene carbonate containing 1.0 mol dm<sup>-3</sup> LiClO<sub>4</sub> (1.0 M LiClO<sub>4</sub>/PC). The correlation between the capacitance and the BET (Brunauer-Emmett-Teller) specific surface area of the microporous ACFs showed the nonlinearity due to strong ion-sieving of micropores. The double-layer capacitance of the meso/macroporous ACFs was higher than the microporous ACF, because the ion-sieving effect of micropores was relaxed by the presence of meso/macropores. The relaxation by the meso/macropores was enhanced for the cation adsorption or the high current density measurement. These results confirm that the presence of many meso/macropores promotes the formation of an effective double layer or fast transfer of ions in the microporous structure.  
© 2002 The Electrochemical Society. [DOI: 10.1149/1.1481525] All rights reserved.

Manuscript submitted September 21, 2001; revised manuscript received January 25, 2002. Available electronically May 14, 2002.

Recently, Electric double-layer capacitors (EDLCs)<sup>1,2</sup> have been proposed as the subpower source for hybrid electric vehicles (HEVs) because of their higher power density (larger than 1000 W kg<sup>-1</sup>), high cycle-efficiency, and long lifetime. However, since the energy density of the EDLC is only several Wh kg<sup>-1</sup> and therefore much lower than that of rechargeable batteries, the capacitance of EDLCs has to be increased. The practical electrode material for the EDLC is porous carbon such as activated carbons. The high capacitance (100-200 F g<sup>-1</sup>) is due to high specific surface area (>1000 m<sup>2</sup> g<sup>-1</sup>) due to many micropores (2 nm > pore width<sup>3</sup>).

In general, it is believed that there is a proportional correlation between the specific surface area and the EDLC of activated carbons, as based on the following equation<sup>1,4,5</sup>

$$C = \int \frac{\epsilon_0 \epsilon_r}{\delta} dS \quad [1]$$

where  $C$  is specific capacitance,  $\epsilon_0$  is permittivity in vacuum,  $\epsilon_r$  is relative permittivity of the double layer,  $\delta$  is thickness of the double layer, and  $S$  is surface area. This equation is derived from an ideal capacitor consisting of a solid dielectric layer between two parallel-plate electrodes such as practical ceramic or film capacitors (condenser). However, some researchers have reported nonlinearity of the double-layer capacitance on surface area.<sup>6-14</sup> This may be due to the dimension of ion or solvent in electrolyte and the pore size distribution (PSD) of activated carbons. In particular, mesopores (2 nm < pore width < 50 nm<sup>3</sup>) or macropores (pore width > 50 nm<sup>3</sup>) should not be ignored because they can influence the permeation of electrolyte to microporous structure or the mobility of ions in the pore.

In the meantime, activated carbon fiber (ACF) is known to have a sharp PSD of micropores without larger pores such as mesopores or macropores.<sup>15,16</sup> Generally, ACF is manufactured by carbonization and gas activation of carbon precursor such as phenolic resin fiber, pitch fiber, and polyacrylonitrile fiber. However, uncommon ACFs containing many mesopores (or macropores) were recently prepared by blending an activation catalyst with phenolic resin<sup>17</sup> or isotropic pitch.<sup>18</sup> These characteristic ACFs with mesopores and macropores are a suitable material for investigating the influence of

the large pores on the double-layer capacitance, because the conventional ACF prepared without an activation catalyst has few meso/macropores.

In our previous work,<sup>19,20</sup> the double-layer capacitance of the ACFs with meso/macropores (referred to as meso/macroporous ACF) was compared with that of the conventional ACFs (referred to as microporous ACF). As a result, it was revealed that the double-layer capacitance of ACFs was enhanced by the presence of meso/macropores. However, some significant properties of the meso/macroporous ACFs (*e.g.*, such as the influence of activation catalysts on the capacitance, the difference in the capacitance between cation and anion, and the rate property) have not been reported yet. In this paper, the properties of the double-layer capacitance for the meso/macroporous ACFs are discussed in detail in order to confirm the effect of meso/macropores on the double-layer capacitance.

### Experimental

**Preparation of meso/macroporous ACFs.**—It is well known that activated carbons containing mesopores or macropores can be obtained through the activation process of carbon materials under the presence of an activation metal catalyst.<sup>17,18</sup> There are two ways for loading the catalyst in the pure carbon matrix: one is the impregnation method, in which the activation catalyst is impregnated by the immersion of carbon materials in the solution containing the catalyst chemicals. Another one is known as the blending method,<sup>17,21</sup> indicating the mixing of carbon precursor and catalyst precursor before carbonization. The latter has the advantage that micropores in activated carbons are not closed with the loaded catalyst. In the present study, the characteristic ACFs with meso/macropores were prepared by a blending method using nickel as the activation catalyst. The detailed procedure is described in previous papers.<sup>19,20</sup> Novolak-type phenolic resin (obtained from Gun-Ei Chemical Industry Co., Ltd., Japan) and bis(2,4-pentanedionate)nickel(II) dihydrate (nickel acetylacetonate dihydrate, (CH<sub>3</sub>COCHCOCH<sub>3</sub>)<sub>2</sub>Ni·2H<sub>2</sub>O, Wako Chemical, Japan) were used as the carbon precursor and the catalyst precursor for steam activation, respectively. The percentage of nickel in the raw materials was 0.1 wt %. The samples containing Ni species or without an agent were referred to as 0.1 Ni-ACF [activation duration (min)] or Ref-ACF [activation duration (min)], respectively.

An acid treatment of 0.1 Ni-ACFs was conducted to discuss the influence of nickel species in 0.1 Ni-ACFs on carbon matrix, pore structure, or double-layer capacitance. In this paper, 1.0 mol dm<sup>-3</sup> H<sub>2</sub>SO<sub>4</sub> aqueous solution was used as the acid. The 0.1 Ni-ACFs

\* Electrochemical Society Active Member.

<sup>z</sup> E-mail: ssiraishi@chem.gunma-u.ac.jp

were immersed in 1.0 M H<sub>2</sub>SO<sub>4</sub> aq for 12 h. The samples treated with the acid were washed twice in pure water to eliminate residual H<sub>2</sub>SO<sub>4</sub> and dried at 60°C for 24 h.

**Characterization of ACFs.**—X-ray diffraction (XRD, RINT 2100V/PC, Rigaku, Japan) analysis was used to investigate the carbon matrix structure of the ACFs and the chemical state of nickel in 0.1 Ni-ACFs. The N<sub>2</sub> adsorption/desorption measurement at 77 K was conducted using an N<sub>2</sub> adsorption/desorption system (BELSORP28SA, BEL Japan, Inc.) to characterize the pore structure of the ACFs. The Brunauer-Emmett-Teller specific surface area (BET-SSA) was calculated from the BET plot of the N<sub>2</sub> adsorption isotherm in the low relative pressure between 0 and 0.05 to prevent the overestimation of surface area due to micropore filling effect.<sup>22</sup> The PSD of mesopores was obtained by the Dolimore-Heal (DH) method using the adsorption branch.<sup>23</sup> In the DH method, morphology of mesopore is considered to be cylindrical shape. The average micropore width was estimated by the Dubinin-Radushevich (DR) equation.<sup>24,25</sup> The surface morphology or the surface composition of ACFs was observed with scanning electron microscopy (SEM, JSM-5300, JEOL, Japan) or X-ray photoelectron spectroscopy (XPS, ESCA5600, Ulvac-Phi, Inc., Japan), respectively.

**Measurement of electric double-layer capacitance of ACFs.**—A composite pellet electrode was prepared from ground ACF (0.05 g), acetylene black (BET-SSA: 53 m<sup>2</sup> g<sup>-1</sup>, Denki Kagaku Kogyo Co., Japan), and polytetrafluoroethylene binder (PTFE 6J, DuPont-Mitsui Fluorochemicals Co., Ltd., Japan). The ratio of ACF (dried at 200°C for 2 h under ~1 Pa), acetylene black, and binder in the electrode was 86:10:4 wt %, respectively. Ti mesh was used as the current collector for the composite electrode. A standard three-electrode cell was used to measure the double-layer capacitance of a single ACF electrode. The counter electrode was lithium metal foil. The reference electrode was lithium metal connected with nickel wire. The measurement of the double-layer capacitance was conducted under galvanostatic conditions in propylene carbonate (PC) containing 1.0 mol dm<sup>-3</sup> LiClO<sub>4</sub> electrolyte (1.0 M LiClO<sub>4</sub>/PC, Kishida Chemical Co., Ltd., Japan). The upper limited potential for the measurement was 4.0 V vs. Li/Li<sup>+</sup>, and the lower was 2.0 V vs. Li/Li<sup>+</sup>. The concentration of water as an impurity in the electrolyte was estimated to be <30 ppm by a Karl-Fischer moisture titrator (MKC-510N, Kyoto Denshi Kogyo, Japan). In this paper, the process of electrons passing from (to) the carbon electrode is referred to as a positive (negative) process. The double-layer capacitance was calculated by the amount of electricity passed during a positive or negative process according to the following equation

$$C = it/m\Delta V \quad [2]$$

where  $C$  is the electric double-layer capacitance (F g<sup>-1</sup>),  $i$  current (A),  $t$  the positive (or negative) duration (s),  $m$  the weight of ACF in the electrode (g), and  $\Delta V$  is the potential change during the positive (or negative) process (V) (2 V in this study). The capacitance calculated by Eq. 2 corresponds to the specific gravimetric electric double-layer capacitance of the ACFs.

## Results and Discussion

**Matrix condition of ACFs.**—Figure 1a and b shows the XRD patterns of Ref-ACFs and 0.1 Ni-ACFs, respectively. In the case of Ref-ACFs, all patterns were typical of amorphous carbon, composed of a broad 002 line and 10 line attributed to micrographite structure. The intensive background around  $2\theta = 10\text{--}15^\circ$  was concerned with the small-angle X-ray scattering derived from the presence of many micropores in the carbon matrix. The X-ray diffraction (XRD) patterns of 0.1 Ni-ACFs showed three metallic nickel lines (111, 200, and 220), in addition to the same broadened lines of amorphous carbon as Ref-ACF. This result indicates that the elemental nickel in 0.1 Ni-ACFs was present as metallic nickel particles in the amorphous carbon structure. Catalytic graphitization by nickel was not

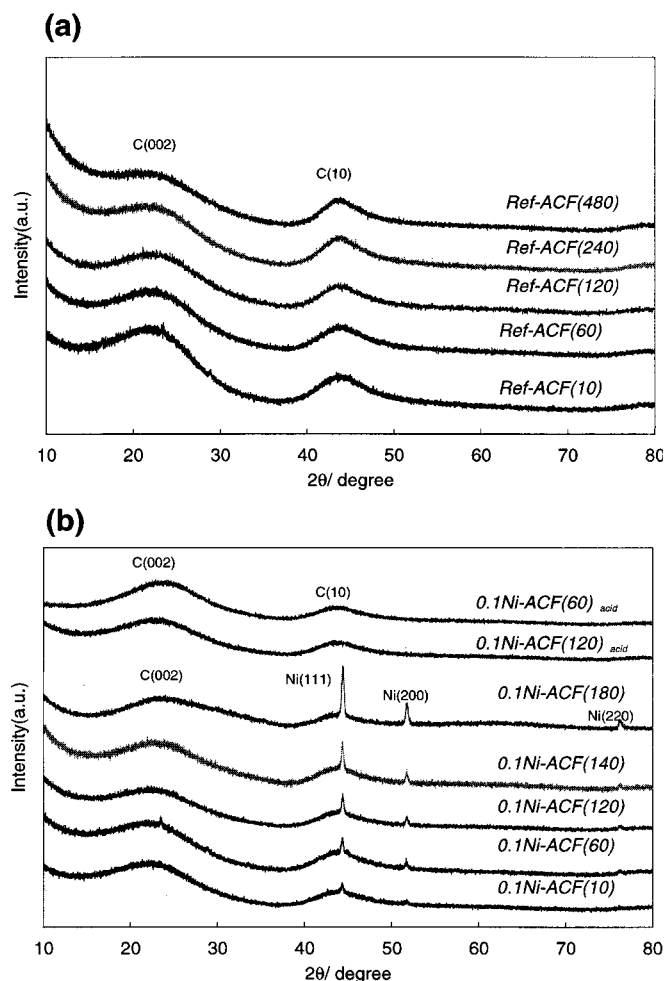


**Figure 1.** XRDs of (a) Ref-ACFs and (b) 0.1 Ni-ACFs. The sample “0.1 Ni-ACF(60)<sub>acid</sub>” or “0.1 Ni-ACF(120)<sub>acid</sub>” is the 0.1 Ni-ACF(60) or 0.1 Ni-ACF(120) after immersion in 1.0 M H<sub>2</sub>SO<sub>4</sub> aq for 12 h.

observed for these 0.1 Ni-ACFs. When the activation duration was longer, the peak intensity of metallic nickel became larger and the full width at half maximum (fwhm) of metallic nickel became shaper. Applying the Scherrer equation to the 111 line of metallic nickel in 0.1 Ni-ACF(10), 0.1 Ni-ACF(120), or 0.1 Ni-ACF(180), the crystallite size was estimated to be about 39, 51, or 62 nm, respectively. These suggested that the metallic nickel particles grew during the activation process. The two XRD patterns in the top of Fig. 1b were obtained from the 0.1 Ni-ACF(60) and the 0.1 Ni-ACF(120) after the immersion process in 1 M H<sub>2</sub>SO<sub>4</sub> aq (the sample names are 0.1 Ni-ACF(60)<sub>acid</sub> and 0.1 Ni-ACF(120)<sub>acid</sub>). No nickel peaks were observed in these XRD patterns. Therefore, it can be said that the loaded nickel particles in 0.1 Ni-ACFs are exposed on the surface of the carbon matrix.

**Pore structure and surface of ACF.**—The N<sub>2</sub> adsorption/desorption isotherms of Ref-ACFs and 0.1 Ni-ACFs are shown in Fig. 2. In all isotherms of the Ref-ACFs, a large amount of N<sub>2</sub> was remarkably adsorbed at low relative pressure (<0.1 P/Ps), while the N<sub>2</sub> adsorption was saturated at middle and high P/Ps. Therefore, the adsorption behavior of the Ref-ACFs is regarded as a typical Type I isotherm for microporous carbon. The drastic increment in adsorption at the low relative pressure is due to the micropore-filling effect.<sup>3,22</sup> The Ref-ACF prepared with longer activation has a larger amount of N<sub>2</sub> adsorption. This shows that the microporous structure in ACF is developed with the activation duration. In the case of 0.1

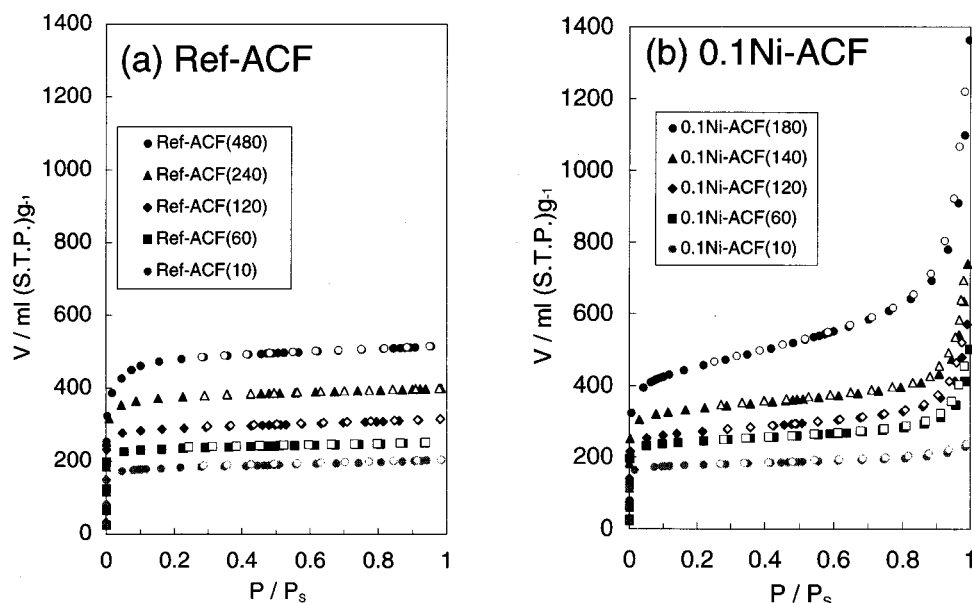


**Figure 2.**  $N_2$  adsorption and desorption isotherms at 77 K for (a) Ref-ACFs and (b) 0.1 Ni-ACFs: (●, ▲, ◆, ■, ●) adsorption isotherms, (○, △, ◇, □, ○) desorption isotherms.

Ni-ACFs, drastic adsorption of  $N_2$  was observed at low relative pressure as well as the case in Ref-ACFs. However, the amount of adsorbed  $N_2$  of 0.1 Ni-ACFs gradually increased even in the region of middle  $P/P_s$  and markedly increased again in the region of high  $P/P_s$ , such as  $>0.8 P/P_s$ . The adsorption increasing in the region of middle and high  $P/P_s$  was observed more distinctly in the 0.1 Ni-ACFs prepared with longer activation duration. This adsorption behavior can be attributed to the capillary condensation of  $N_2$  in the mesopores (or macropores) and multilayer adsorption on the mesopores or the macropores. The PSD of the mesopores for 0.1 Ni-ACFs and Ref-ACFs calculated by the DH method are shown in Fig. 3. The former has few mesopores except for small pore size ( $\sim 2$  nm) closed to micropores, while the latter has great pore volume in the whole mesopore region. The amount of mesopore volume in the range 10–40 nm pores became much larger in the Ni-ACF prepared with longer activation. This indicates that the nickel catalyst is effective in the formation of mesopores with relatively large pore size.

The BET-SSA (corresponding to the total SSA of ACFs) and the DH pore volume ( $V_{\text{meso}}$ , corresponding to the total pore volume of mesopores in the ACFs) are summarized in Table I. In both Ref-ACFs and 0.1 Ni-ACFs, the BET-SSA was higher as the activation duration was extended. This means that the pore structure in the ACFs is well developed with longer activation time. The mesopore volume in Ref-ACFs was increased slightly through the activation, while the mesopore volume in 0.1 Ni-ACFs was markedly changed by the activation from 0.10 to 0.86  $\text{mL g}^{-1}$ . 0.1 Ni-ACF had larger

mesopore volume compared to Ref-ACF with almost the same BET-SSA. The micropore volume ( $V_{\text{micro}}$ ) and the average micropore width ( $w_{\text{micro}}$ ) estimated by the DR equation<sup>22,23</sup> are also summarized in Table I.  $V_{\text{micro}}$  and  $w_{\text{micro}}$  became larger with longer activation duration, regardless of the Ref-ACF series and 0.1 Ni-ACF series. There was little difference between  $V_{\text{micro}}$  and  $w_{\text{micro}}$  between Ref-ACF and 0.1 Ni-ACF with almost identical BET surface area [for example, Ref-ACF(120) vs. 0.1 Ni-ACF(120), and Ref-ACF(480) vs. 0.1 Ni-ACF(180)]. These results suggested that the surface area of mesopores in 0.1 Ni-ACFs does not contribute significantly to the total surface area, although the mesopore volume of 0.1 Ni-ACFs is significant in the total pore volume ( $V_{\text{meso}} + V_{\text{micro}}$ ). Consequently, 0.1 Ni-ACFs can be considered to be characteristic ACFs containing both numerous mesopores and micropores, and the large specific surface area of 0.1 Ni-ACFs is due to the developed micropore structure as well as Ref-ACFs.

The BET surface area, the pore volume, and the micropore width of 0.1 Ni-ACF(60)<sub>acid</sub> or 0.1 Ni-ACF(120)<sub>acid</sub> are also shown in Table I. The mesopore volume of these 0.1 Ni-ACFs was increased slightly by the immersion in the acid. This increment in the mesopore volume can be due to the removal of the metallic nickel particles in the 0.1 Ni-ACFs that contribute to blocking the entrance of some pores. In contrast, the BET surface area,  $V_{\text{micro}}$ , and  $w_{\text{micro}}$  were slightly smaller than before the acid treatment. These suggest some contraction of micropore structure by the acid treatment. How-

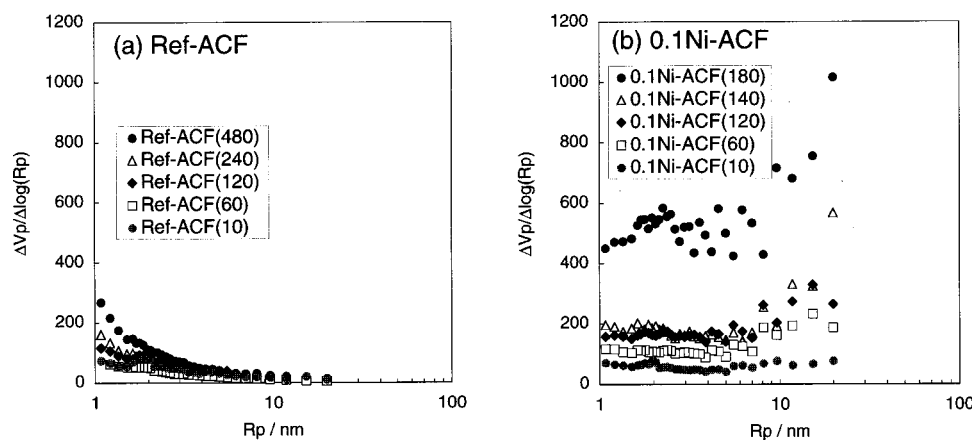


**Figure 3.** PSDs for the mesopore region of (a) Ref-ACFs and (b) 0.1 Ni-ACFs(180), calculated by the DH method.  $R_p$  is pore radius,  $V_p$  pore volume.

**Table I. BET-SSA, mesopore volume, average micropore width, and micropore volume of various ACFs.<sup>a</sup>**

Sample <sup>b</sup>	BET-SSA (m <sup>2</sup> g <sup>-1</sup> )	V <sub>meso</sub> (mL g <sup>-1</sup> )	V <sub>micro</sub> (mL g <sup>-1</sup> )	w <sub>micro</sub> (nm)
Ref-ACF(10)	650	0.06	0.28	0.64
Ref-ACF(60)	930	0.03	0.37	0.73
Ref-ACF(120)	1150	0.08	0.47	0.85
Ref-ACF(240)	1480	0.09	0.60	0.94
Ref-ACF(480)	1780	0.16	0.73	1.07
0.1 Ni-ACF(10)	710	0.10	0.28	0.69
0.1 Ni-ACF(60)	960	0.21	0.38	0.74
0.1 Ni-ACF(60) <sub>acid</sub> <sup>c</sup>	920	0.23	0.36	0.72
0.1 Ni-ACF(120)	1050	0.30	0.42	0.83
0.1 Ni-ACF(120) <sub>acid</sub> <sup>c</sup>	1000	0.32	0.39	0.79
0.1 Ni-ACF(140)	1290	0.35	0.52	0.88
0.1 Ni-ACF(180)	1660	0.86	0.69	1.06

<sup>a</sup> BET-SSA calculated by BET plot in the region of 0-0.05 P/Ps.

w<sub>micro</sub>: Average micropore width calculated from DR method.

V<sub>micro</sub>: Pore volume of micropore calculated from DR method.

V<sub>meso</sub>: Pore volume of mesopore (1.6-40 nm) calculated from DH method of adsorption branch.

<sup>b</sup> Number in parenthesis indicates the activation duration (min).

<sup>c</sup> The 0.1 Ni-ACFs after the immersion in 1.0 M H<sub>2</sub>SO<sub>4(aq)</sub> for 12 h.

ever, since these changes in the pore structure before and after the acid treatment are essentially small, it can be said that the removal process of metallic nickel particles essentially does not influence the pore structure of the 0.1 Ni-ACFs.

Figure 4 is the SEM images of Ref-ACF(480), 0.1 Ni-ACF(60), and 0.1 Ni-ACF(180). Many macropores with pore size smaller than 1 μm and many mesopores with relatively large pore size were observed in these 0.1 Ni-ACFs, especially 0.1 Ni-ACF(180). No macropores or no mesopores were observed in the Ref-ACF(480). Therefore, it can be seen that the steam activation under nickel species also produces many macropores in addition to mesopores in ACF.

The yield and the bulk density of electrodes for Ref-ACFs and 0.1 Ni-ACFs are shown in Table II. The yield and the electrode bulk density became smaller with longer activation duration in both Ref-ACFs and 0.1 Ni-ACFs. The yield and the electrode bulk density of

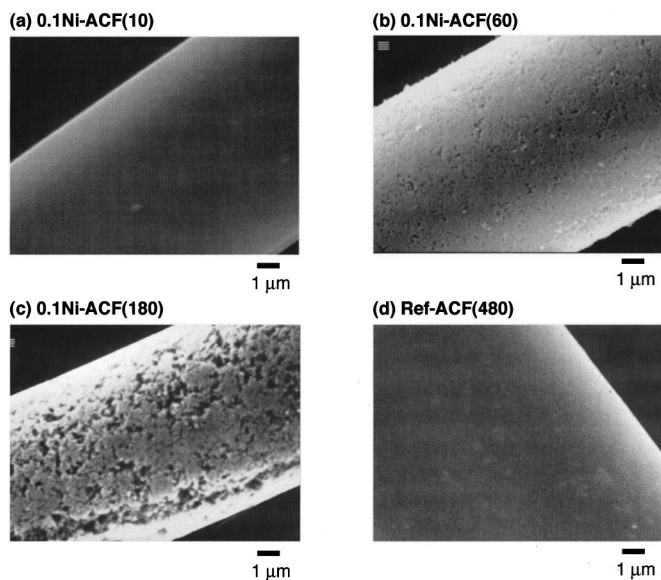


**Figure 4.** SEMs of (a) 0.1 Ni-ACF(10), (b) 0.1 Ni-ACF(60), (c) 0.1 Ni-ACF(180), or (d) Ref-ACF(480).

**Table II. Yield of various ACFs, bulk density of composite electrode, and surface oxygen/carbon atomic ratio of various ACFs.**

Sample	Yield (%)	d <sup>a</sup> (g cm <sup>-3</sup> )	O/C <sup>b</sup>
Ref-ACF(10)	52	1.00	0.07
Ref-ACF(60)	45	0.87	0.08
Ref-ACF(120)	41	0.85	0.06
Ref-ACF(240)	35	0.74	0.06
Ref-ACF(480)	23	0.68	0.06
0.1 Ni-ACF(10)	47	0.85	0.07
0.1 Ni-ACF(60)	29	0.62	0.05
0.1 Ni-ACF(120)	16	0.54	0.04
0.1 Ni-ACF(140)	15	0.43	0.04
0.1 Ni-ACF(180)	5	0.38	0.05

<sup>a</sup> d: Bulk density of the composite electrode composed of ACF, acetylene black, and binder (86:10:4 wt %).

<sup>b</sup> O/C: Surface oxygen/carbon atomic ratio estimated by XPS.

0.1 Ni-ACF were lower than those of Ref-ACF with almost the same BET-SSA. The lower yield and the lower bulk density are due to the catalytic activation (gasification) of nickel. This is in a good agreement with the results of pore analysis by N<sub>2</sub> adsorption and SEM observation.

The surface oxygen/carbon atomic ratios of the ACFs, estimated by the XPS analysis, are also shown in Table II. These results revealed little difference in surface oxygen content between Ref-ACF and 0.1 Ni-ACF. The XPS O 1s spectra and the C 1s spectra in Ref-ACF were similar to those in 0.1 Ni-ACFs (these spectra are not shown in this paper), which also indicates little difference in the kinds of surface functionalities between Ref-ACFs and 0.1 Ni-ACFs. Therefore, these facts suggest that the effect of surface functionalities on double-layer capacitance does not need to be considered in this paper.

**Electric double-layer capacitance of ACF.**—Figure 5a and b shows the potential-time curves (chronopotentiograms) for Ref-ACFs and 0.1 Ni-ACFs in 1.0 M LiClO<sub>4</sub>/PC electrolyte. The electrode potential of Ref-ACF(240), Ref-ACF(480), 0.1 Ni-ACF(120), 0.1 Ni-ACF(140), and 0.1 Ni-ACF(180) was changed linearly by the amount of electricity passed for the positive or negative process. Therefore, these ACF electrodes are regarded as a polarizable electrode with a constant capacitance. Any plateaus derived from electrochemical reactions such as nickel dissolution or oxidation were not observed in the curves of these 0.1 Ni-ACFs. Moreover, the chronopotentiograms of 0.1 Ni-ACF(60)<sub>acid</sub> and 0.1 Ni-ACF(120)<sub>acid</sub> in Fig. 5c were similar to those of 0.1 Ni-ACF(60) and 0.1 Ni-ACF(120), so it can be seen that the metallic nickel particles loaded on 0.1 Ni-ACFs do not affect the double-layer capacitance. On the other hand, the profiles of Ref-ACF(60), Ref-ACF(120), and 0.1 Ni-ACF(60) were distorted triangles with a variable gradient. Since the slope of the curve corresponds to the capacitance, it follows that the double-layer capacitance of these ill-activated ACF electrodes depends on the electrode potential during the positive or negative process. The dependence of the capacitance on the electrode potential may be due to the difference in the capacitance between the anion adsorption/desorption process and the cation adsorption/desorption process. The slopes of the potential-time curves of Ref-ACF(10) and 0.1 Ni-ACF(10) were very steep, so the capacitance of these ACFs is very small. The capacitance was estimated by Eq. 2 to determine the relationship between the BET-SSA and the double-layer capacitance in detail.

Figure 6a is the correlation between the BET-SSA and the electric double-layer capacitance in 1.0 M LiClO<sub>4</sub>/PC, obtained from the positive process. This correlation was very similar to that obtained from the same ACFs in PC solution containing tetraethyl ammonium salt.<sup>24,25</sup> The capacitance of each ACF electrode during the positive process was nearly the same as that obtained from the negative process, which means that the coulombic efficiency was

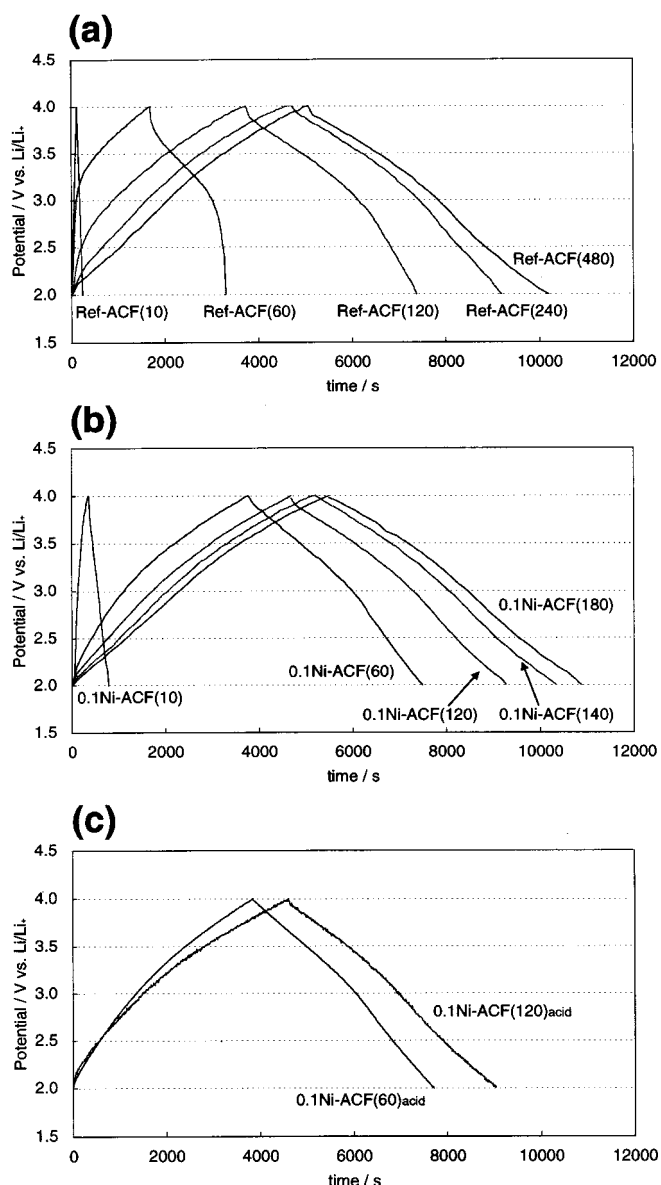


**Figure 5.** Potential-time curves (chronopotentiograms) for (a) Ref-ACFs, (b) 0.1 Ni-ACFs, and (c) 0.1 Ni-ACFs<sub>acid</sub> in 1.0 mol dm<sup>-3</sup> LiClO<sub>4</sub>/PC. Galvanostatic method (40 mA g<sup>-1</sup>), potential range 2-4 V vs. Li/Li<sup>+</sup>.

almost 100%. The correlation for 0.1 Ni-ACFs<sub>acid</sub> was also plotted in Fig. 6a. These data confirm that the loaded nickel particles in 0.1 Ni-ACFs do not influence the double-layer capacitance.

Both the correlations for Ref-ACFs and 0.1 Ni-ACFs revealed that the double-layer capacitance was not linearly proportional to the BET-SSA. Since these ill-activated ACFs [e.g., Ref-ACF(10) or 0.1 Ni-ACF(10)] have narrower micropores, <0.7 nm pore width, the very small capacitance of these ACFs can be attributed to the difficulty in forming an effective double layer or the low mobility of the ion in the narrow micropores. The Stokes radius is well known as an index of the solvated ion size. The Stokes radius of Li<sup>+</sup> cation or ClO<sub>4</sub><sup>-</sup> anion in PC can be estimated with the following equation<sup>26,27</sup>

$$r_s = \frac{z_i^2 F^2}{x \pi N_A \lambda_0 \eta} = \frac{0.492 \times 10^2 z_i^2}{x \lambda_0 \eta} \quad [3]$$

where  $r_s$  is the Stokes radius (nm),  $z_i$  is the charge number of ion,  $F$  the Faraday constant,  $N_A$  Avogadro's constant,  $\lambda_0$  the single ion

limiting molar conductivity (S cm<sup>2</sup> mol<sup>-1</sup>),  $\eta$  is solvent viscosity (cP), and  $x$  is 4 in the case of ClO<sub>4</sub><sup>-</sup>, 5.7 in the case of Li<sup>+</sup>.<sup>27</sup>

With Eq. 2 and the single ion limiting molar conductivities of Li<sup>+</sup> and ClO<sub>4</sub><sup>-</sup> in PC,<sup>27</sup> the Stokes radius of Li<sup>+</sup> cation or ClO<sub>4</sub><sup>-</sup> anion in PC solution was estimated to be 0.41 or 0.26 nm. Thus the solvated Li<sup>+</sup> cation size (0.82 nm) or ClO<sub>4</sub><sup>-</sup> anion size (0.52 nm) is very close to the micropore width of Ref-ACF(10) or 0.1 Ni-ACF(10). Therefore, if the Stokes radius can be applied to the discussion about the ions in micropores, "ion-sieving effect" of narrow micropores, something like "molecular sieving," is a good explanation of very small capacitance of the ill-activated ACFs (the nonlinearity of capacitance to surface area). Soffer's group also reported the ion-sieve phenomenon of micropores in ACF.<sup>14</sup>

In the case of the better-activated ACFs with high surface area, the double-layer capacitance of 0.1 Ni-ACFs was higher than that of Ref-ACFs with almost the same BET-SSA. Particularly, the higher capacitance of 0.1 Ni-ACFs was prominent in the region of 900-1200 m<sup>2</sup> g<sup>-1</sup> BET-SSA [e.g., Ref-ACF(60) vs. 0.1 Ni-ACF(60), or Ref-ACF(120) vs. 0.1 Ni-ACF(120)]. In the previous section, it has already been revealed that the mesopores in the 0.1 Ni-ACF series were developed better than those in the Ref-ACFs, although there was little difference in the micropore structure for both series of samples from the viewpoint of the average micropore width and the micropore volume. Consequently, this advantage of the capacitance of 0.1 Ni-ACFs can be attributed to the presence of many mesopores (or macropore), which assists the transfer of ions through the microporous structure or the permeation of nonaqueous electrolyte into the pores to form the electric double layer on the pore surface. Furthermore, these mesopores effects can be expected to be weaker in ACFs with sufficiently large micropores to ions. In fact, Fig. 6a indicates that the advantage of the mesopores for the capacitance was not so effective in the ACFs with large micropore width [e.g., Ref-ACF(480) and 0.1 Ni-ACF(180)] as that of the ACFs with 900-1200 m<sup>2</sup> g<sup>-1</sup> BET-SSA. This result also confirms the ion sieving of micropores and the mesopore effect.

The double-layer capacitance seems to be saturated in the high surface area such as higher than 1200 m<sup>2</sup> g<sup>-1</sup> for both Ref-ACFs and 0.1 Ni-ACFs. It cannot be explained with the ion-sieving effect because the micropore width is large enough for the ions to move in the ACFs. One of the reasons for the saturation may be the overestimation of SSA with the BET model for activated carbons with high surface area.<sup>22,28</sup> However, the possibility of the overestimation should be avoided using the BET plots at low relative pressure,<sup>22</sup> as described in the experimental section. Therefore, the capacitance saturation of the ACFs with high surface area is caused by another factor. The variation of the surface carbon structures by the activation<sup>29</sup> (e.g., such as the ratio of the edge plane and the basal plane of micrographite) may also affect the correlation between the capacitance and the surface area. Randin and Yeager already reported the difference in the specific capacitance per surface area between the edge plane and the basal plane of highly oriented pyrolytic graphite (HOPG).<sup>30</sup>

**Cation capacitance and anion capacitance of ACF.**—In the previous section, it was seen that the pore size distribution of ACFs effectively affects the double-layer capacitance in 1.0 M LiClO<sub>4</sub>/PC electrolyte. Based on the comparison between the pore size and the solvated ion size, the difference in capacitance between cation and anion should be also observed if the cation size is different from the anion. The solvated Li<sup>+</sup> cation (0.82 nm) is larger than the solvated ClO<sub>4</sub><sup>-</sup> (0.52 nm), so it can be expected that the advantage of 0.1 Ni-ACFs for the anion adsorption/desorption capacitance is weaker than that for cation adsorption/desorption. The evaluation of each adsorption capacitance can be conducted by separation of chronopotentiograms at the initial potential before the measurement (namely, pzc: the immersion potential of electrode<sup>31</sup>) as shown in Fig. 7. The initial potential of each ACF electrode was between 3.0-3.1 V vs. Li/Li<sup>+</sup>. The chronopotentiogram in the upper potential region to the initial potential reflects the capacitance of the anion adsorption/

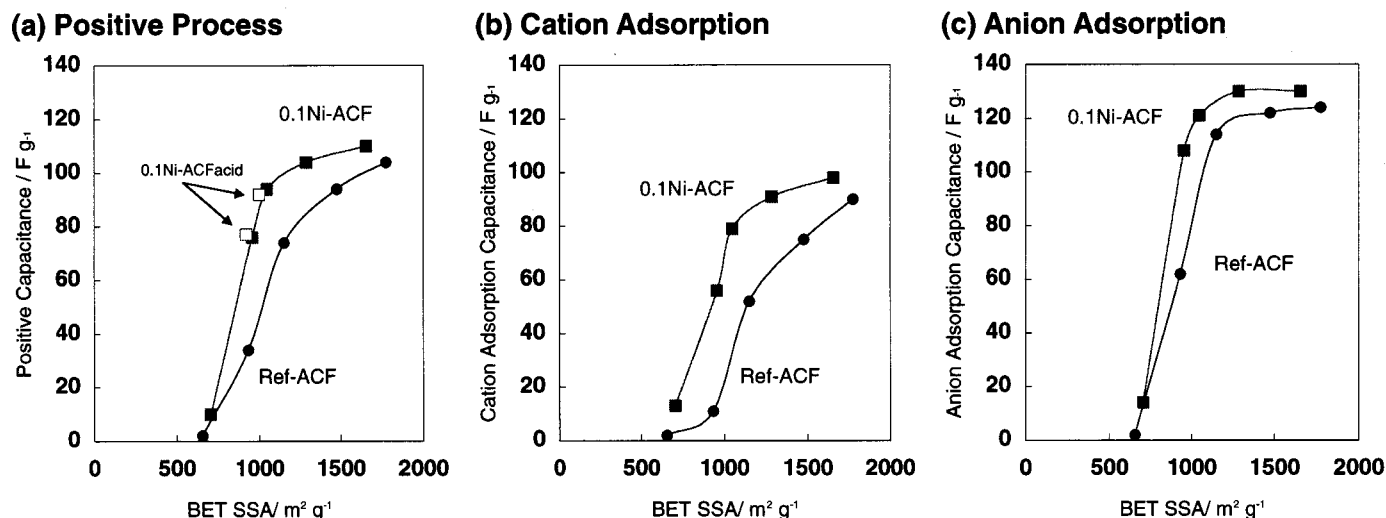


**Figure 6.** Correlation between BET-SSA and electric double-layer capacitance during positive process for Ref-ACFs and 0.1 Ni-ACFs in 1.0 mol dm<sup>-3</sup> LiClO<sub>4</sub>/PC. Galvanostatic method (40 mA g<sup>-1</sup>), positive process 2 V → 4 V vs. Li/Li<sup>+</sup>. (□) Obtained from 0.1Ni-ACFs<sub>acid</sub>.

desorption, since the ACF electrode must compensate the lack of electrons with negative charge of anion in electrolyte. Similarly, the lower potential region to the initial potential corresponds to the capacitance of the cation adsorption/desorption because of the excess electrons. These suggest that each capacitance shown in Fig. 6a is an average capacitance of cation desorption and anion adsorption.

Thus, the cation adsorption capacitance was calculated from the potential-time curve at potentials lower than 3 V vs. Li/Li<sup>+</sup> during the negative process. The anion adsorption capacitance was also evaluated from the curve at potentials higher than 3 V vs. Li/Li<sup>+</sup> during the positive process. These capacitances are shown in Fig. 6b and c, respectively. These results revealed that the cation capacitance of Ref-ACFs was smaller than the anion capacitance, and that the advantage of 0.1 Ni-ACF in the capacitance was more prominent for the cation adsorption capacitance than the anion adsorption. These results suggest the following two points. First, the solvated Li<sup>+</sup> cation cannot go easily through microporous structure compared with the ClO<sub>4</sub><sup>-</sup> anion. Second, the mesopores can assist Li<sup>+</sup> cation better to move in microporous structure than ClO<sub>4</sub><sup>-</sup> anion. Therefore, the ion sieving of micropores or the assistance of mesopores to the ion moving in the microporous structure is more effective for the Li<sup>+</sup> cation as larger ions.

*Rate property of electric double-layer capacitance of ACF.*—As mentioned in the introduction, one of the merits of EDLC is high power density, so the rate property of the double-layer capacitance is significant. Figure 8 is the dependence of the double-layer capacitance on the current density for Ref-ACFs and 0.1 Ni-ACFs. Since higher current density causes more serious IR drop derived from electrode resistance, each capacitance in Fig. 8 was estimated from the chronopotentiograms only in the region of 2.25–3.75 V vs. Li/Li<sup>+</sup> to eliminate the influence of the IR drop on the capacitance evaluation. The double-layer capacitance of 0.1 Ni-ACFs during the negative process decreased slightly with high current density, while that of Ref-ACFs reduced markedly at higher current density except for Ref-ACF (240). These results suggest that the ions in the microporous structure with meso/macropores can follow the large electric perturbation such as high current density. According to Morita's results,<sup>32</sup> one kind of mesoporous ACF also showed a good rate property in EC/DMC (ethylene carbonate-dimethyl carbonate) mixture solution containing LiBF<sub>4</sub>. Thus, meso/macroporous ACFs can be considered as a promising material for high-power EDLCs. However, the bulk electrode density of 0.1 Ni-ACF is considerably smaller than that of Ref-ACFs, and the yield of 0.1 Ni-ACFs is also lower. Therefore, the advantage of 0.1 Ni-ACFs should be consid-

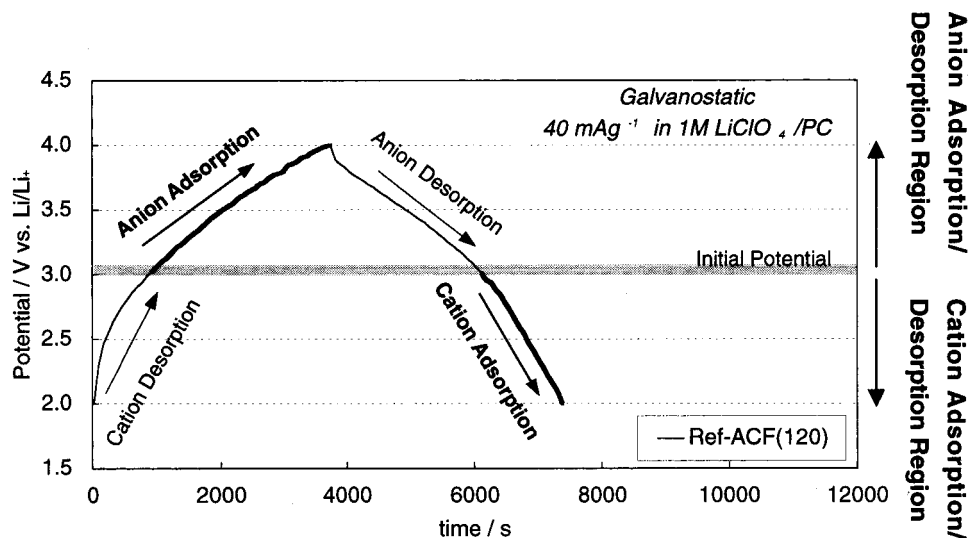


**Figure 7.** Schematic illustration for evaluation of anion adsorption capacitance and cation adsorption capacitance from chronopotentiograms of ACF electrode. The chronopotentiogram in the upper (lower) potential region than the initial potential reflects the anion (cation) adsorption/desorption.

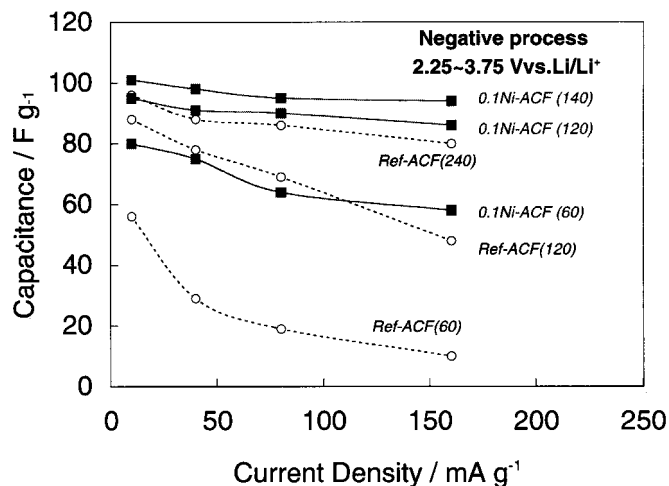


**Figure 8.** Dependence of electric double-layer capacitance (negative process) on current density for various Ref-ACFs and 0.1 Ni-ACFs in 1.0 mol dm<sup>-3</sup> LiClO<sub>4</sub>/PC. Galvanostatic method (10, 40, 80, 160 mA g<sup>-1</sup>), negative process 4 V → 2 V vs. Li/Li<sup>+</sup>. Each capacitance was calculated from each chronopotentiogram in the region of 2.25-3.75 V vs. Li/Li<sup>+</sup> to eliminate the influence of IR drop.

ered on the viewpoint of volumetric capacitance and the cost when applying these mesoporous ACFs to a practical EDLCs.

### Conclusion

Meso/macroporous ACFs that contain many meso/macropores in addition to micropores were prepared from carbonization and steam activation of a phenolic resin fiber blended with activation catalyst of nickel. The gravimetric electric double-layer capacitance of the meso/macroporous ACFs and the conventional microporous ACFs was measured in 1.0 M LiClO<sub>4</sub>/PC using a three-electrode cell. As a result, the following points were clarified about the correlation between the double-layer capacitance and the pore structure.

1. In both cases of the meso/macroporous ACFs and the microporous ACFs, the double-layer capacitance could not be explained simply with the linearity to the specific surface area. This nonlinearity is due to the low permeability of nonaqueous electrolyte to the microporous structure or the low mobility of the ion in the narrow micropores of ACFs.

2. The meso/macroporous ACFs showed higher double-layer capacitance than the microporous ACFs. This result suggests that the presence of many mesopores (or macropores) promotes the formation of an effective double layer or the transfer of ions in the microporous structure. This effect is more prominent when a cation with large size in the electrolyte, such as Li<sup>+</sup> cation, is adsorbed/desorbed.

3. The capacitance of the meso/macroporous ACFs was higher even at high current density measurement compared with that of the microporous ACFs.

These results show how significant PSD in activated carbons and ion size in electrolyte are for the improvement of the double-layer capacitance. Therefore, the correlation of the double-layer capacitance with the pore structure of activated carbons and the physicochemical properties of electrolyte must be investigated in more detail using other samples in the future (for example, ACFs with various pore size distributions prepared from other activation catalysts, other electrolytes with various quaternary onium salts, etc.).

### Acknowledgment

A part of this study was financially supported by Industrial Technology Research Grant Program in 2001 from the New Energy and Industrial Technology Development Organization (NEDO) of Japan.

Gunma University assisted in meeting the publication costs of this article.

### References

- B. E. Conway, *Electrochemical Super Capacitors*, Kluwer Academic/Plenum Publishers, New York (1999).
- A. Nishino, *J. Power Sources*, **60**, 137 (1996).
- S. J. Gregg and K. S. W. Sing, *Adsorption, Surface Area and Porosity*, Academic Press, London (1982).
- I. Takahashi, A. Yoshida, and A. Nishino, *Electrochemistry*, **56**, 892 (1988).
- T. Morimoto, K. Hiratsuka, Y. Sanada, and K. Kurihara, *J. Power Sources*, **60**, 239 (1996).
- H. Shi, *Electrochim. Acta*, **41**, 1633 (1996).
- D. Qu and H. Shi, *J. Power Sources*, **74**, 99 (1998).
- S. Iwasaki, Y. Okusako, M. Miyahara, and M. Okazaki, *Kagaku Kogaku Ronbunshu*, **23**, 512 (1997) (in Japanese).
- C. Lin, J. A. Ritter, and B. N. Popov, *J. Electrochem. Soc.*, **146**, 3639 (1999).
- H. Nakagawa, A. Shudo, and K. Miura, *J. Electrochem. Soc.*, **147**, 38 (2000).
- Y. Sakata, A. Muto, M. A. Uddin, N. Yamada, C. Marumo, S. Ibaraki, and K. Kojima, *Electrochem. Solid-State Lett.*, **3**, 1 (2000).
- S. Yoon, J. Lee, T. Hyeon, and S. M. Oh, *J. Electrochem. Soc.*, **147**, 2507 (2000).
- S. Shiraishi, H. Kurihara, H. Tsubota, A. Oya, S. Soneda, and Y. Yamada, *Electrochem. Solid-State Lett.*, **4**, A5 (2001).
- G. Salitra, A. Soffer, L. Eliad, Y. Cohen, and D. Aurbach, *J. Electrochem. Soc.*, **147**, 2486 (2000).
- M. Suzuki, *Carbon*, **32**, 577 (1994).
- S. K. Ryu, *High Temp.-High Press.*, **22**, 345 (1990).
- A. Oya, S. Yoshida, J. Alcaniz-Monge, and A. Linares-Solano, *Carbon*, **33**, 1085 (1995).
- H. Tamai, K. Kakii, Y. Hirota, T. Kumamoto, and H. Yasuda, *Chem. Mater.*, **8**, 454 (1996).
- S. Shiraishi, H. Kurihara, and A. Oya, *Carbon Science*, **1**, 133 (2001).
- S. Shiraishi, H. Kurihara, and A. Oya, *Electrochemistry*, **69**, 440 (2001).
- J. Przepiorski and A. Oya, *J. Mater. Sci. Lett.*, **17**, 679 (1998).
- K. Kaneko, C. Ishii, M. Ruike, and H. Kuwabara, *Carbon*, **30**, 1075 (1992).
- D. Dollimore and G. R. Heal, *J. Appl. Chem.*, **14**, 109 (1964).
- M. M. Dubinin and H. F. Stoeckli, *J. Colloid Interface Sci.*, **75**, 34 (1980).
- M. E. Merraoui, H. Tamai, H. Yasuda, T. Kanata, J. Mondori, K. Nadai, and K. Kaneko, *Carbon*, **36**, 1769 (1998).
- Y. Matsuda, H. Nakashima, M. Morita, and Y. Takasu, *J. Electrochem. Soc.*, **128**, 2552 (1981).
- M. Ue, *J. Electrochem. Soc.*, **141**, 3336 (1994).
- H. Marsh, *Activated Carbon Compendium*, H. Marsh, Editor, Elsevier, Oxford (2001).
- P. L. Walker, Jr., F. Rusinko, Jr., and L. G. Austin, *Advances in Catalysis*, Vol. XI, D. D. Eley, P. W. Selwood, and P. B. Weisz, Editors, p. 136, Academic Press, Inc., New York (1959).
- J. P. Randin and E. Yeager, *J. Electrochem. Soc.*, **118**, 711 (1971).
- H. Tobias and A. Soffer, *J. Electroanal. Chem.*, **148**, 221 (1983).
- M. Morita, S. Watanabe, M. Ishikawa, H. Tamai, and H. Yasuda, *Electrochemistry*, **69**, 462 (2001).